ESC-TR-99-065

Project Report
NOAA-3 (R-1)

HgCdTe Detector Responsivity and GOES Instrument Calibration

W.E. Bicknell

12 March 1993
Revised 17 May 2000

Lincoln Laboratory
MASSACHUSETTS INSTITUTE OF TECHNOLOGY
LEXINGTON, MASSACHUSETTS

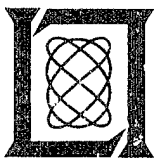

Prepared for the National Oceanographic and Atmospheric Administration under Air Force Contract F19628-90-C-0002.

This report is based on studies performed at Lincoln Laboratory, a center for research operated by Massachusetts Institute of Technology. The work was sponsored by the National Oceanographic and Atmospheric Administration under Air Force Contract F19628-95-C-0002.

The ESC Public Affairs Office has reviewed this report, and it is releasable to the National Technical Information Service, where it will be available to the general public, including foreign nationals.

This technical report has been reviewed and is approved for publication.

FOR THE COMMANDER

Gary Tatungian
Administrative Contracting Officer
Plans and Programs Directorate
Contracted Support Management

MASSACHUSETTS INSTITUTE OF TECHNOLOGY
LINCOLN LABORATORY

HgCdTe DETECTOR RESPONSIVITY AND GOES INSTRUMENT CALIBRATION

W.E. BICKNELL
Group 96

PROJECT REPORT NOAA-3 (R-1)

12 MARCH 1993

Revised 17 MAY 2000

LEXINGTON MASSACHUSETTS

ABSTRACT

A model is developed for the reponsivity of HgCdTe detectors employed in the GOES Sounder and Imager instruments. Response non-linearity is related to the calibrated radiometric accuracy of the instruments. The model, in the form of a computer code, could be utilized to expedite pre-launch calibration of GOES satellite instruments and to provide confidence in GOES in-orbit calibration procedures.

ACKNOWLEDGMENTS

This report describes work I completed in the late Summer of 1992. The work was motivated by my participation in the GOES Calibration Task Force. Technical interchanges at meetings with Bill Bryant, chairman, and with fellow Task Force members contributed much to the direction and results.

I appreciate Mike Weinreb for explaining NOAA calibration and data reduction procedures, for discussions about calibration, and for encouraging pursuit of the analysis. I acknowledge helpful discussions on the topic of HgCdTe detector physics with Dave Spears, Rich Schoolar, and Marion Reine.

Jack Lifsitz and Dan Mooney have provided valuable editorial review.

TABLE OF CONTENTS

LIST OF ILLUSTRATIONS

LIST OF TABLES

1. INTRODUCTION

Weather information to be provided by the GOES satellite requires the satellite's instruments to be well calibrated. Instrument calibration requires testing prior to launch in a space simulation chamber. Measurements are taken over a wide range of chamber radiometric conditions and instrument temperatures. Pre-launch calibration testing is relatively time consuming and costly.

A model of the responsivity of the GOES instruments could expedite pre-launch calibration testing; however, a model that includes instrument response non-linearity has not been developed. Non-linearity in GOES instrument response is attributable to the HgCdTe detector and detector preamplifier.

This report describes an analysis of the non-linear responsivity of the GOES Sounder and Imager instruments and sets forth a collection of equations, or model, given in the form of a computer code that could be utilized to facilitate pre-launch calibration of GOES satellite instruments and to provide confidence in GOES in-orbit calibration procedures.

1.1 BACKGROUND

An accuracy goal of ±1K in scene brightness temperature makes the GOES instruments sensitive to small non-linearity in the relationship between incident sensed irradiance and the measured voltage, or counts. This can be illustrated by differentiating the Planck function with respect to the temperature, T,

$$\frac{dN}{N} = \left(\frac{c_2}{\lambda T}\right)^2 \left(\frac{\mathrm{Exp}\left(\frac{c_2}{\lambda T}\right)}{\mathrm{Exp}\left(\frac{c_2}{\lambda T}\right) - 1}\right) \frac{dT}{T} \qquad (1)$$

where N is spectral radiance, c_2=14391 μm-K, and λ is the wavelength in μm. A plot of this expression for the fractional radiance versus wavelength is shown in Figure 1 for a ±1K uncertainty in T.

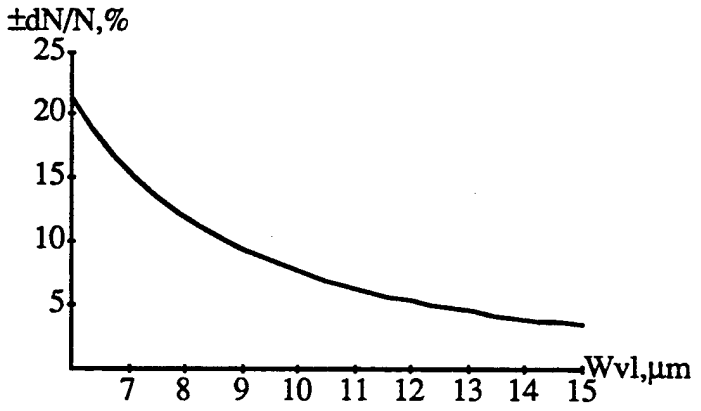

Figure 1. Radiance uncertainty vs wavelength for ±1K uncertainty in 300°K scene brightness.

From Figure 1 it is observed that, particularly at longer wavelengths covered by the instruments, the uncertainty in N must be small ($\leq 5\%$) to achieve a ± 1K data accuracy. Only part of the radiance uncertainty budget is assigned to the uncertainty in calibration. Thus, very small calibration uncertainties, on the order of a few %, are significant.

The calibration equation converts measured counts (Δcounts), taken with respect to a space or zero radiance reference, to scene radiance. The equation is imbedded in NOAA Operational Ground Equipment (OGE) computer software. The OGE computer software converts data to radiance values from the Δcount data telemetered to ground from the orbiting satellite.

In-orbit calibration for GOES is planned to be the same as that used for the AVHRR: Each instrument will be commanded to sequentially observe space and an onboard blackbody target. This provides data for determination of two coefficients in the calibration equation. For the AVHRR the coefficients are the offset and linear terms.

Consider a plot of a calibration equation shown in Figure 2: The plotted equation resulted from a fit to pre-launch calibration data taken for the 10.3 -11.3 μm channel of an Advanced Very High Resolution Radiometer(AVHRR) used in the NOAA-7 satellite[Ref 1]. The instrument employs HgCdTe photo-conductive detectors and electronic circuitry that is similar to the circuitry in the GOES instruments. A non-linearity is evident: The responsivity of the AVHRR decreases as the radiance value increases. To fit the data the calibration equation requires use of a constant offset, linear, and quadratic coefficient to relate radiance to Δcounts.

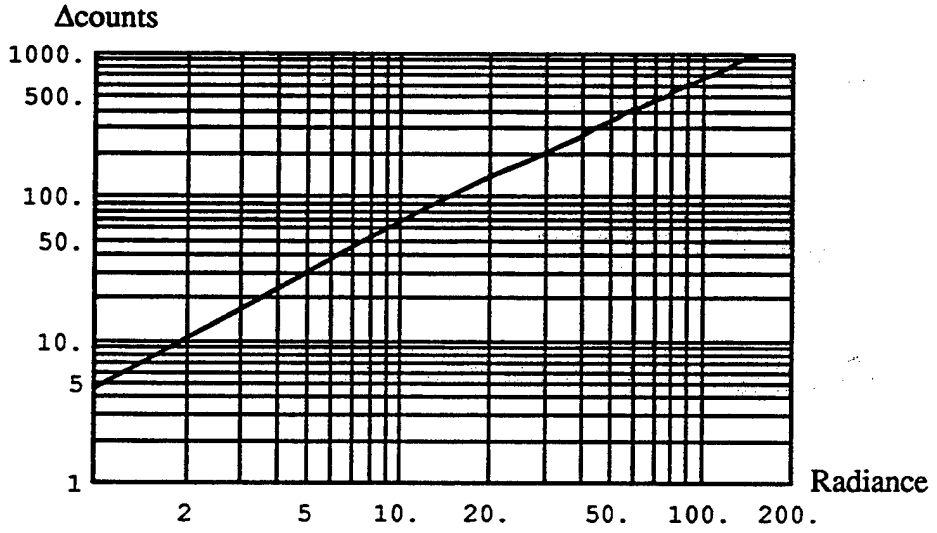

Figure 2. ΔCounts vs radiance for channel 4 of the NOAA-7 AVHRR at a baseplate temperature of 10C.

Coefficients of the AVHRR calibration equation have been found to depend on the background flux impinging upon the detector. Radiometric background flux on a AVHRR instrument is influenced by the instrument baseplate temperature. In Figure 2 the baseplate temperature is 10C. At different baseplate temperatures the calibration curve coefficients are different by several percent.

The AVHRR quadratic coefficient is inferred from the in-orbit instrument baseplate temperature and a pre-orbit ground test data base. The data base was collected by operating the AVHRR at various baseplate temperatures in a space simulation chamber. The method employed by NOAA to determine the AVHRR quadratic non-linearity coefficient is described by Mike Weinreb et al.[Ref 2].

The GOES instruments require in-orbit calibration updates over a range of fore-optics baffle temperatures. During certain seasons the instruments carried aboard the geo-synchronous GOES satellite will be subject to radiation heat loading from the sun. At such times, the sun appears just out of the field-of-view and partially illuminates the instrument's fore-optics baffle structure. The sun's illumination will increase the fore-optics baffle temperature and, thereby, change the radiometric background power on the detectors.

The GOES satellite instruments require in-orbit calibration updates over a range of detector temperatures. Non-linear instrument responsivity due to HgCdTe detectors will be a function of the detector operating temperature. A quadratic calibration coefficient which accounts for the response non-linearity will also depend on the detector operating temperature. Temperature of AVHRR detectors is kept constant; however, GOES detectors will operate at several temperatures(from 94 to 105K) over the course of a year and over the satellite's lifetime.

Correcting calibration coefficients using measurements taken in orbit requires a pre-orbit chamber test data base that encompasses the range of temperature variations expected in orbit. Employing a model to extrapolate between instrument temperatures could facilitate calibration equation coefficient correction using a minimum pre-orbit chamber test data base.

The planned GOES chamber calibration procedure involves measuring the response of an instrument for a number ($\leq$10) of incident flux levels. Each flux level is obtained by changing the temperature of a black body in the chamber. Allowing the temperature to stabilize at each level consumes considerable chamber test time.

The number of test flux levels is driven by a requirement to fit the measurements to a calibration equation. One contribution to the number of flux levels that must be used is an uncertainty in the form of the calibration equation. A model of the calibration equation could remove this uncertainty and, thereby, permit use of fewer flux levels.

If N_l is the number of flux level measurements, N_c the number of coefficients, σ_d the data percent precision, and σ_f the fit percent uncertainty, then the number of flux levels could be chosen in accordance with approximately

$$\sigma_f \approx \frac{\sigma_d}{\sqrt{N_l - N_c}}.$$

E.g., for a three-coefficient calibration equation and suitably small σ_d, a minimum of $\approx$4-5 flux levels might be adequate.

1.2 NON-LINEARITIES

There are two causes of instrument response non-linearity: The first is the bias circuit and preamplifier used to sense the changes in conductance. The second is the departure of

HgCdTe photo-conductors from linearity in response to impinging radiometric flux. This distinction is of interest because in the past response non-linearity has been individually attributed to each cause. As will be discussed, it is due to both.

1.2.1 CIRCUIT NON-LINEARITY

Figure 3 illustrates GOES instrument detector and detector preamplifier circuitry. The circuit employs a photo-conductive detector that, along with a connecting wire resistance, exhibits a 100 to 200 Ohm resistance, R_d, in one arm of a bridge network The bridge network serves as the input to a low noise operational amplifier.

The resistance values R_a and R_c in the second arm of the bridge are chosen to approximately zero-balance the voltage input to the preamplifier under a quiescent operating condition.

The bridge resistance in series with the detector, R_b, is used to control the detector bias current caused by the bias voltage, V_o. The bias voltage is ≈10 Volts and typical bias currents employed are ≈1 to 2 mA. This results in a resistance value of ≈5000 to 10,000 Ohms. Because the value of R_b dominates the resistance of the bridge arm the influence of the detector resistance, Rd, on the bias current is small.

The detector's resistance is a function of the power, P_p, due to incident radiometric flux. Small changes in the value of R_d due to changes in P_p cause small changes in R_d at the balanced bridge input to the preamplifier. These changes are sensed and amplified by the preamplifier.

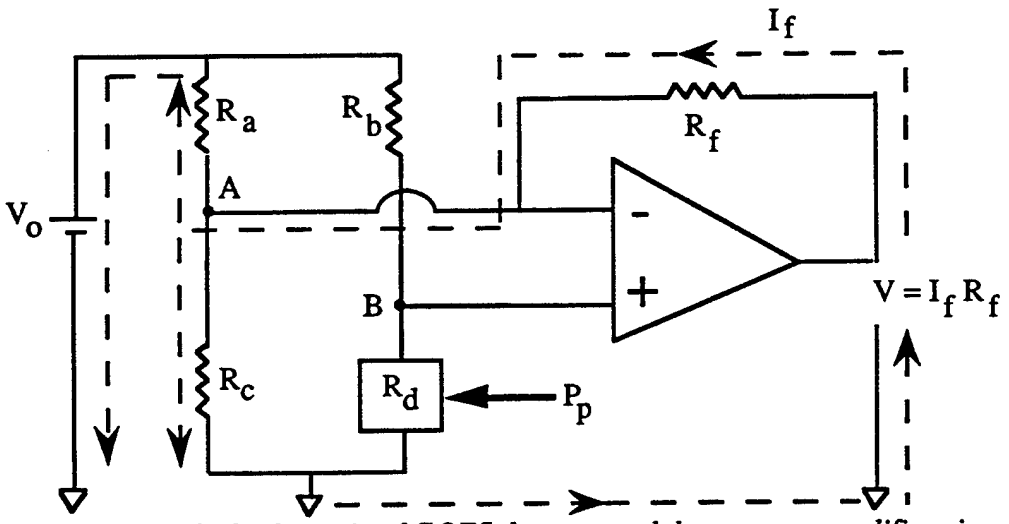

Figure 3. Simplified schematic of GOES detector and detector preamplifier circuit.

The preamplifier employs a feedback resistor, R_f. The summing junction in the feedback loop is the negative input to the preamplifier and is tied to node A shown in Figure 3. The feedback current, I_f, divides at node A and returns to the preamp through either R_a and V_o, or through R_c. The feedback current drives the voltage at node A to be equal to that at node B. Solving V_A=V_B gives the preamplifier output voltage, V

$$V = V_o \frac{R_f(R_a + R_c)}{R_a R_c}\left(\frac{R_d(P_p)}{R_b + R_d(P_p)} - \frac{R_c}{R_a + R_c}\right) \quad (2)$$

Because typically $R_b >> R_d$ and $R_a >> R_c$, Eq.(2) can be written as

$$V \cong \frac{V_o}{R_b}\frac{R_f}{R_c}\left(R_d(P_p) - R_c\right) \quad (3)$$

The bridge arm resistance, R_d, is the sum of the resistance of the cooled photo-conductor and that of a thin connecting wire resistance. The thin connecting wire in series with each contact of the detector provides thermal impedance isolation of the preamplifier circuitry from the cryogenic cooler that controls the detector temperature.

If R_w is the wire resistance and $\mathbf{R_d}$ is the actual cooled detector resistance, then

$$R_d = R_w + \mathbf{R_d} \quad (4)$$

The value of R_w is in the 50-75 Ohm range and is significant with respect to the value of $\mathbf{R_d}$.

A photo-conductor exhibits a conductance, $\mathbf{G_d}=1/\mathbf{R_d}$, that equals the sum of a constant, quiescent conductance plus a photo-sensitive conductance. For an ideal photo-conductor, the photo-sensitive conductance is linearly proportional to impinging radiometric flux. Circuit non-linearity in GOES instruments is attributed to the fact that the value of V, indicated by Eqs. (2) and (3), is proportional to R_d rather than $\mathbf{G_d}$. The preamplifier circuit would create a small response non-linearity even if an ideal photo-conductor were employed.

1.2.2 DETECTOR NON-LINEARITY

Real photo-conductors exhibit a conductance,$\mathbf{G_d}$, that can change non-linearly in proportion to the incident radiometric flux. Causes of HgCdTe detector photo-conductive non-linearity include:

1) non-ohmic contacts
2) flux dependence of the Auger relaxation time*
3) flux dependence of the surface recombination relaxation time*
4) flux dependence of diffusion and electric-field carrier sweepout.

The non-linearities considered in this analysis are marked with an asterisk.

It is assumed that a detector exhibits ohmic contacts. I.e., it is assumed detector resistance is substantially independent of the direction of charge flow through the detector. During manufacture, detectors are tested for symmetry of resistance to forward and reverse bias to identify and eliminate detectors with non-ohmic contacts.

Flux dependence of diffusion and electric-field carrier sweepout effects can be important, especially at bias voltages higher than typically employed for GOES detectors. However, the effect is difficult to model and is discussed in Section 2.3.

Flux dependence of the carrier relaxation times and carrier sweepout is due to the dependence of the Auger relaxation time(the principal carrier relaxation mechanism), the diffusion coefficient, and the ambipolar mobility on carrier density.

2. MODEL OF CIRCUIT AND DETECTOR NON-LINEARITY

Detector circuit response is set forth as a series expansion in a factor equaling the product of the HgCdTe responsivity and the radiometric scene power incident on a detector. The responsivity of the detector is then taken as a Taylor's series expansion around the quiescent operating point determined by incident background power. The resulting instrument responsivity expression is related to the calibration equation. Finally, physical causes of the detector's non-linear responsivity are briefly described.

2.1 ANALYTIC EXPRESSION FOR RESPONSIVITY

In orbit, a reference voltage is determined with the instrument observing space. Although radiometric flux falls on the detector due to background radiation from the instrument, the "space-look" voltage is used as a reference for zero signal flux incident on the instrument's optical entrance aperture. When the instrument's optical field-of-view is turned to earth the difference voltage,ΔV, between the "space-look" reference and the observed voltage is used to ascertain the earth scene's radiance.

Data transmitted to NOAA for processing by the OGE is a stream of digital counts. The counts are derived from an A/D converter onboard the satellite. It is assumed that the A/D converter is linear and that its voltage resolution is small compared to the required precision of the data. (The A/D resolution error contributes a small random component to the instrument's additive noise.)

If at some time, t, a power, $P_p[t]$, during observation of an earth scene is incident on the detector, then from Eqs.(3) and (4) the preamplifier voltage at time t is given by

$$V(P_p[t]) = \frac{V_o}{R_b}\frac{R_f}{R_c}\{R_w[t]+\mathbf{R_d}(P_p[t]) - R_c[t]\} + V_n[t] \qquad (5a)$$

where $V_n[t]$ is a zero-mean random noise. Similarly, if at time t+t' a power $P_p[t + t']$ from a space reference is incident on the detector then the preamplifier voltage at time t+t' is given by

$$V(P_p[t+t']) = \frac{V_o}{R_b}\frac{R_f}{R_c}\{R_w[t+t']+\mathbf{R_d}(P_p[t+t']) - R_c[t+t']\} + V_n[t+t'] \qquad (5b)$$

The Δvoltage reported, ΔV, is taken to be

$$\Delta V = < V(P_p[t]) - V(P_p[t+t']) > \qquad (6)$$

where the brackets < > denote an ensemble average. It is assumed that Equation (6) simplifies to give

$$\Delta V = \frac{V_o}{R_b}\frac{R_f}{R_c} < (\mathbf{R_d}(P_p[t]) - \mathbf{R_d}(P_p[t+t'])) > \qquad (7a)$$

$$= \frac{V_o}{R_b}\frac{R_f}{R_c}(< \mathbf{R_d}(P_s[t]+P_b[t]) > - < \mathbf{R_d}(P_b[t+t']) >) \qquad (7b)$$

$$= \frac{V_o}{R_b}\frac{R_f}{R_c}(R_d(P_s+P_b) - R_d(P_b)) \qquad (7c)$$

where P_s is the earth scene power incident on the detector and P_b is the quiescent background power from the instrument environment.

Equations (7a)-(7c) indicate in a somewhat formalistic way that random, temporal changes due to noise and variation in circuit parameters are taken to be averaged to zero. In practice, data from both earth scenes and space reference scenes can be averaged. It is assumed averaging achieves a reduction of the random and temporal noise to the extent that it does not contribute to calibration error.

Imprecision of processed in-orbit instrument data must be small compared to the required accuracy of the radiometric product. To be limited in radiometric accuracy by only a small instrument non-linearity is, indeed, a significant achievement.

Equations (7) indicate that $\Delta V \to 0$ as $P_s \to 0$. However, this has not been observed for the AVHRR or the SN02 and SN03 GOES instruments[Ref 3,4]. Chamber test data indicate a small offset. I.e., it was observed that $\Delta V \to \Delta V_{offset}$ as $P_s \to 0$ where ΔV_{offset} is a small, but nonetheless significant, value in comparison to the ΔV associated with the NEDN and NEDT of the instruments.

The AVHRR instruments were tested at the ITT space chamber in Ft. Wayne, IN. If some periodic electromagnetic interference (EMI) were present or if $P_b[t] \neq P_b[t+t']$ then such an offset might be anticipated. An offset might also be expected if, because of spurious sources of radiation in the test chamber at ITT, the reference value for P_s is not zero as it is assumed to be.

If an offset exists due to the instrumentation, then the offset should be included in the calibration equation irrespective of a model. (It is not included in the model developed from this analysis.) If, on the other-hand, the offset is a peculiarity of the tests and is not exhibited in orbit, it is an aberration that should not be included in the calibration equations. It is not easy to resolve this issue with the planned two-datum, in-orbit calibration correction procedure. The offset term presents an issue that is important to calibration; it is recommended that it be further investigated.

Eq.(7c) is in accord with the author's understanding of how GOES instruments were designed to perform in orbit.

The value of G_d depends on the power falling on the detector as well as detector material parameters:

$$G_d(P_p) = g_{ss} + q\mu_e\left(n_o + \frac{\lambda_p \eta(\lambda_p)\, \tau(P_p)\, P_p}{h\, c\, HWL} \right)\frac{H\,W}{L_e} = \frac{1}{R_d(P_p)} \qquad (8)$$

where

P_p = power impinging on detector, Watts, from photons at wavelength λ_p, μm
g_{ss} = surface state shunt conductance, mho

q = charge of electron, Coulomb, h = Planck's constant, Joule-sec, c = velocity of light, μm/sec
H = detector height, cm, W = detector width, cm, L = detector length(along electrodes), cm
detector photo-responsive area = W x L, cm^2, L_e = detector electrical length, cm.
η = quantum efficiency, τ = effective bulk relaxation time, sec
(n_o, p_o) = thermally-generated equilibrium (electron, hole) concentration, #/cm^3
μ_e = electron carrier mobility, cm^2/Volt-sec

The detector parameters g_{ss}, μ_e, n_o, τ, and λ_p depend on the detector operating temperature. For the sake of simplicity, notation conveying this dependence will not be carried. Substituting Eq.(8) into Eq.(7c), setting the gain factor R_f/R_c equal to unity, one obtains for Δvoltage, apart from an overall gain factor that is not pertinent to the analysis,

$$\Delta V = - \frac{\rho(P_b+P_s)\,P_s}{1 + \frac{\rho(P_b+P_s)\,P_s}{I_o}} R_d(P_b) \qquad (9)$$

where $\rho(P_b+P_s)$ is the detector current responsivity given by

$$\rho = \frac{q\lambda_p}{h\,c}\,\eta(\lambda_p)\,\frac{\mu_e\,\tau(P_b+P_s)}{L\,L_e}\,I_o\,R_d(P_b), \text{ Amp/Watt} \qquad (10)$$

and the bias current I_o is given by V_o/R_b.

Equation (9) indicates that ΔV is proportional to the scene power incident on the detector, P_s, apart from a term in the denominator of the right-hand-side that is also proportional to P_s. This denominator term produces a small non-linearity in the response that is attributable to the circuit non-linearity.

For small non-linearity Eq.(9) can be approximated by

$$\Delta V \cong - \rho(P_b+P_s)\;R_d(P_b)\,P_s\left[1 - \frac{\rho(P_b+P_s)}{I_o}P_s + \left(\frac{\rho(P_b+P_s)}{I_o}\right)^2 P_s^2\right] + \ldots\ldots \qquad (11)$$

Equation (11) indicates that the circuit non-linearity may be accounted for by a polynomial correction factor in P_s. It is important to note that this does not include a detector response non-linearity. The detector non-linearity lies in the detector current responsivity, $\rho(P_b+P_s)$. If the detector response non-linearity is small it can be approximated by the first terms of a Taylor's Series

$$\rho(P_b+P_s) = \rho(P_b) + \rho'(P_b)P_s + 0.5\,\rho''(P_b)P_s^2 + \ldots\ldots\ldots \qquad (12)$$

which is a reasonable approximation for $P_s << P_b$. Substituting Eq.(12) into Eq.(9) gives an expression that includes both the circuit and detector responsivity non-linearities:

$$\Delta V \cong -\rho(P_b)\, R_d(P_b)\, P_s\left[1-\left\{\frac{\rho(P_b)}{I_o}-\frac{\rho'(P_b)}{\rho(P_b)}\right\}P_s-\left\{\left(\frac{\rho(P_b)}{I_o}\right)^2+\frac{2\rho'(P_b)}{I_o}-0.5\,\frac{\rho''(P_b)}{\rho(P_b)}\right\}P_s^2\right] \quad (13)$$

Equation (13) is a simple expression for a response non-linearity in P_S up to cubic order. Note there are two contributions to the coefficients of the non-linear terms: One is traceable to the circuit non-linearity and one is attributable to the detector response non-linearity. In the cubic coefficient the effects are cross-coupled. Since $\rho'(P_b)$ is negative (ρ decreases with increasing P_b) the circuit and detector non-linearity effectively add together in the coefficient for the quadratic term.

2.2 INSTRUMENT RESPONSIVITY AND THE CALIBRATION EQUATION

It is useful to examine how the responsivity of the instrument, Eq.(13), relates to a non-linear calibration equation used by NOAA in the OGE.

Apart from an overall electronics gain factor, which is set to unity for this analysis, the ΔV responsivity of the instrument to power on the detector, P_S, can be expressed as

$$\Delta V = \alpha_1 P_S + \alpha_2 P_S^2 + \alpha_3 P_S^3 + \ldots\ldots\ldots\ldots \quad (14a)$$

where the coefficients (α_1, α_2, ...) are taken from Eq.(13). A calibration equation in terms of ΔV and power on the detector can be expressed in the form

$$P_S = \beta_1 \Delta V + \beta_2 \Delta V^2 + \beta_3 \Delta V^3 + \ldots\ldots\ldots\ldots \quad (14b)$$

Substituting Eq.(14a) into (14b) and solving for the relation between the coefficients gives, to third order in ΔV and P_S

$$\beta_1 = \frac{1}{\alpha_1}, \quad \beta_2 = -\frac{\alpha_2}{(\alpha_1)^3} \quad \text{and} \quad \beta_3 = \frac{\dfrac{2(\alpha_2)^2}{\alpha_1} - \alpha_3}{(\alpha_1)^4} \quad (15)$$

Equation (15) indicates that, for small corrections about a linear relationship, one may examine the non-linearity of calibration either in the instrument responsivity formulation or the calibration equation formulation. Results may be mapped from one to the other via relationships of the coefficients of a series expansion in either formulation.

The OGE converts Δcounts reported from an instrument channel into an observed spectral radiance. To describe this process consider two variables (x,y) defined as

$$P_s \equiv 10^{-3}\left(A_o \Omega_o \tau_o \Delta\nu\right) y = \kappa_p\, y, \quad y \text{ in } \frac{mW}{m^2 - Sr\text{-}cm^{-1}} \quad (16a)$$

where

y = instrument channel measured spectral radiance

κ_p = instrument channel spectral radiance to detector scene power conversion factor

A_o = instrument entrance aperture area, m^2

Ω_o = instrument IFOV, Sr

$\Delta\nu$ = instrument effective bandpass, cm^{-1}

τ_o = instrument optical transmission

and

$$\Delta V \equiv \left(\Delta Va/_d\right) x = \kappa_v x , \qquad x \text{ in } \Delta\text{counts} \tag{16b}$$

where

x = instrument channel reported Δcounts

$\kappa_v = \Delta V_{a/d}$, instrument A/D (Δvoltage-to-counts) conversion ratio

The calibration equation used by the OGE is of the form

$$y = b_1 x + b_2 x^2 + b_3 x^3 + \ldots\ldots\ldots\ldots \tag{17}$$

Utilizing Eqs.(16a) and (16b) and comparing Eq.(17) with Eq.(14b) it is found that

$$b_1 = \frac{\kappa_v}{\kappa_p}\beta_1 , \qquad b_2 = \frac{\kappa_v^2}{\kappa_p}\beta_2 \qquad \text{and} \qquad b_3 = \frac{\kappa_v^3}{\kappa_p}\beta_3 \tag{18}$$

It is possible to simply relate the OGE calibration equation coefficients to the coefficients of Eq.(14b). It is notationally convenient to minimize extraneous parameters that vary from channel-to-channel. (The instrument electronic gain is incorporated in the coefficient κ_v.) In this analysis the β coefficients of Eq. (14b) are examined.

From Eqs. (13), (16) and (18), the coefficients b_1 and b_2 are given by

$$b_1 \equiv -\left[\frac{\Delta Va/_d}{10^{-3}\left(A_o\Omega_o\tau_o\,\Delta\nu\right)}\right]\frac{1}{\rho\,R_d} \tag{19a}$$

$$b_2 \equiv +\left[\frac{\left(\Delta Va/_d\right)^2}{10^{-3}\left(A_o\Omega_o\tau_o\,\Delta\nu\right)}\right]\left[\frac{\rho(P_b)}{I_o} - \frac{\rho'(P_b)}{\rho(P_b)}\right]\frac{1}{(\rho R_d)^2} \tag{19b}$$

Equations (19a) and (19b) suggest that the dependence of the coefficients in the OGE calibration equation on background power and temperature can be assessed from detector and detector-preamplifier testing. For example, the product ($\rho\,R_d$) is the voltage responsivity in Volts/Watt. This quantity is measured to ascertain the suitability of manufactured detectors for meeting specification. The detector resistance is also measured using low resistance connecting wires. These measurements are routinely carried out under controlled detector current bias, I_o, a single background power, P_b, and at several detector temperature conditions. The change of

detector responsivity with background, $\rho'(P_b)$, can be determined by measuring the responsivity at two or more controlled background flux levels.

Present measurements might be extended over anticipated instrument operating conditions in bias current, detector temperature, and background power. The results could be analyzed using Eqs. (19) to indicate the effects of the detector and preamplifier circuit performance on the calibration equation before selection of detectors and assembly into an instrument. (The test dewar and set-up would have to accurately reproduce the background flux, signal flux, and temperature that the detectors experience in-orbit.)

2.3 DETECTOR RESPONSE NON-LINEARITY

The detector response non-linearity is primarily due to the influence of a photo-excited carrier density on the re-combination or relaxation time,τ , of photo-excited carriers. Equations that describe detector physics are given in Appendix A.

The major factor contributing to HgCdTe response non-linearity is dependence of the Auger relaxation time,τ_A, on carrier density

$$\tau = \tau_A A_1 = \frac{2(n_i)^2 \tau_{Ai}}{(n_o + p_o + n_p)(n_o + n_p)} A_1 \qquad (20)$$

where

n_i = intrinsic electron density, cm^{-3}
n_o = equilibrium electron density, cm^{-3}
p_o = equilibrium hole density, cm^{-3}
n_p = photo-excited carrier density, cm^{-3}
τ_{Ai} = intrinsic Auger relaxation time($n_p = 0$ and $n_o=p_o=n_i$), Sec
$A_1 = A_1(n_p)$ surface recombination reduction factor.

For a steady-state incident radiometric power, P_p, the steady-state photo-excited carrier density, n_p, is given by

$$n_p = \frac{\eta \lambda_p \tau P_p}{hc H A_d} \qquad (21)$$

The detector's photo-sensitive conductivity is proportional to n_p which, through Eq.(21), is also proportional to P_p. However, from Eq.(20) it is seen that, as n_p approaches a density nearing n_o, the relaxation time will tend to decrease. Through Eq.(21) the decreasing relaxation time decreases the responsivity of the photo-sensitive conductivity to Pp. This leads to a non-linearity in the response to P_p.

The factor A_1 is dependent on n_p through the carrier-dependent diffusion coefficient of HgCdTe material and also influences the non-linearity, although less significantly than τ_A.

Diffusion and electric-field induced carrier sweepout also affect the responsivity of the photo-sensitive conductivity to P_p. These mechanisms influence responsivity, $\rho(P_S)$, as a function of the position between detector electrodes and tend to reduce the small-signal, linear responsivity of a detector. The reduction of the small-signal, linear responsivity due to these mechanisms is described in an appendix of the NOAA Detector Team Final Report[Ref 5]. To the author's knowledge, the influence of these mechanisms on the non-linearity of the detector response has not been reported in the literature.

Modeling the responsivity of a detector affected by diffusion and electric field sweepout requires considering $n_p \rightarrow n_p(x)$, $\tau_A(n_p) \rightarrow \tau_A(n_p(x))$, and $\rho(P_S) \rightarrow \rho(x,P_S)$,where x is a distance along the axis between electrodes. This is difficult to analyze and model; however, experimentally measuring $\rho(x,P_S)$ provides an evaluation of diffusion and electric-field induced carrier sweepout effects. A uniform $\rho(x,P_S)$ indicates absence of effects. LIRIS measurements indicate $\rho(x,P_S)$ becomes just noticeably non-uniform at bias currents of 2.0-3.0 mA or larger. At a bias current of 1.0 mA, no spatial non-uniformity could be discerned[Ref 6].

The analysis ignores diffusion and electric-field induced carrier sweepout. It should be applicable to GOES detectors having bias currents up to ≈2.0- 3.0 mA. Pursuit of the effects of diffusion and electric-field induced carrier sweepout on response non-linearity is recommended as a useful addition to the model.

3. DESCRIPTION OF MODEL CALCULATIONS

A computational method used to obtain a solution for the response is described. The solution gives a responsivity, $\Re(P_b,P_s)$, as a function of P_s. The percent change in the small-signal responsivity, $\Re(P_b,0)$, and $\Re(P_b,P_s)$ is defined as a percent non-linearity function $\%NL(P_b,P_s)$. The computed quantities are related to the calibration coefficient parameters described in Section 2. A brief review is given of detector data available to the author at the time the analysis was undertaken.

3.1 ITERATIVE SOLUTION

Considering A_1 a constant and independently determining n_o, p_o, n_i, τ_{Ai}, η, and λ_p for a detector allows one to substitute Eq.(20) into Eq.(21) and obtain a cubic equation for n_p in terms of P_p. This equation has only one real root and produces a solution that is linear in P_p for $n_p/n_o<<1$. The task of the iteration is to find n_p that yields a self-consistent solution to Eqs.(20) and (21).

The iteration commences by first setting $A_1 = 1$, the value of A_1 in the absence of surface recombination effects. Then, a zeroth-order value of n_p is determined from Eq.(21) using a value of τ derived from Eq.(20) with $n_p = 0$. This zeroth-order value of n_p, $n_p[0]$, is used to calculate $A_1(n_p[0])$. The value of $A_1(n_p[0])$ is then treated as a constant and used in the cubic equation that results from the simultaneous solution of Eqs.(20) and (21) just described. The resultant value of n_p, $n_p[1]$, is used to calculate $\tau(n_p[1])$ and $A_1(n_p[1])$. These, in turn, are used to modify the cubic equation which is then solved for an improved estimate, $n_p[2]$.

This process is repeated until the difference between the estimate of $n_p[k]$ and $n_p[k+1]$ becomes suitably small.

3.2 CALIBRATION EQUATION COEFFICIENTS

The iterative procedure is used to compute a voltage, V_b, that is proportional to the preamplifier voltage produced by the background power in accordance with Eq. (2). This calculation ignores the gain factor and bridge offset voltage subtracted from V_b given in Eq.(2).

$$V_b = V_o \left(\frac{R_d(P_b)}{R_b + R_d(P_b)} \right) \tag{22a}$$

A voltage given by the background power plus signal power, V_{bs}, is computed in a similar manner.

$$V_{bs} = V_o \left(\frac{R_d(P_b+P_s)}{R_b + R_d(P_b+P_s)} \right) \tag{22b}$$

A difference voltage, ΔV_{bs}, is evaluated that gives the difference between V_{bs} and V_b and represents the ΔV reported by the instrument in accordance with Eq.(7c).

$$\Delta V_{bs} = V_{bs} - V_b$$

The voltage, ΔV_{bs}, gives a solution from the iterative procedure for the response of an instrument to an incident scene power, P_s, for a given P_b. The voltage responsivity of the instrument is taken to be $\Re(P_b,P_s)$ where

$$\Re(P_b,P_s) = \frac{\Delta V_{bs}}{P_s} \tag{23}$$

The response non-linearity for a given P_b can be envisioned as the deviation of $\Re(P_b,P_s)$ from a straight line when plotted as a function of P_s. It is difficult to quantitatively determine small non-linearities from such a plot. For this reason the computations include a percent non-linearity function, $\%NL(P_b,P_s)$, that compares $\Re(P_b,P_s)$ with $\Re(P_b,0)$.

To calculate $\Re(P_b,0)$ a small-signal voltage, V_{bss}, is calculated as in Eq. (22b) where $P_s \rightarrow P_{ss} = 10^{-10}P_b$,

$$V_{bss} = V_o \left(\frac{R_d([1+10^{-10}]P_b)}{R_b + R_d(P_b)} \right).$$

A ΔV_{bss} is then computed

$$\Delta V_{bss} = V_{bss} - V_b$$

and the small-signal responsivity, $\Re(P_b,0)$, is evaluated as

$$\Re(P_b,0) = \frac{\Delta V_{bss}}{P_{ss}}. \tag{24}$$

The deviation of $\Re(P_b,P_s)$ from $\Re(P_b,0)$ is a measure of the departure of the responsivity from linearity. The percent non-linearity function is defined as

$$\%NL(P_b,P_s) = 100\left(\frac{\Re(P_b,P_s)}{\Re(P_b,0)} - 1 \right) \tag{25}$$

The percent non-linearity can be interpreted in the following way: It is the percent reduction in actual ΔV_{bs} for P_b+P_s compared to the ΔV_{bs} that would occur for P_s due to the small-signal responsivity ($P_s << P_b$) value.

Comparing the results of the calculations with the analytic expression of Eq.(13), gives the correspondences:

$$\Re(P_b,0) \equiv - \rho(P_b)R_d(P_b) \tag{26}$$

and

$$\%NL(P_b,P_s) \equiv -100\left[\left|\frac{\rho(P_b)}{I_o} - \frac{\rho'(P_b)}{\rho(P_b)}\right| P_s - \left|\left(\frac{\rho(P_b)}{I_o}\right)^2 + \frac{2\rho'(P_b)}{I_o} - 0.5\,\frac{\rho''(P_b)}{\rho(P_b)}\right| P_s^2\right] \tag{27}$$

Equation (27) relates the %NL to $\rho(P_p)$ and detector current, I_o.

The percent non-linearity function and $\Re(P_b,0)$ are used to evaluate the effect of the responsivity on the coefficients of the calibration equation. Comparing the calculated quantities to Eq.(14a) leads to the identification

$$\alpha_1 = \Re(P_b,0) \quad \text{and} \quad \alpha_2 = \frac{\%NL}{100\,P_s} \tag{28}$$

Using Equation (15), the values of β_1 and β_2 are evaluated to examine the change of the calibration equation coefficients with temperature and background power.

The non-linearity evaluated by the preceding computations includes both circuit and detector non-linearities. The detector non-linearity, however, is due solely to the change in the carrier relaxation time, τ. To distinguish between circuit and detector non-linearity a $\%NL_\tau$ function is evaluated:

$$\%NL_\tau(P_b,P_s) = 100\left(\frac{\tau(P_b+P_s)}{\tau(P_b)} - 1\right) \tag{29}$$

The $\%NL_\tau$ function gives the contribution of the detector responsivity non-linearity to the overall %NL.

3.3 AVAILABLE DETECTOR DATA

The HgCdTe detectors used in GOES are tested and characterized by the manufacturer and, independently, by ITT before being mounted in a an instrument package. The tests are currently conducted at a single background flux level and do not characterize the detector's non-linearity.

The values of n_o, p_o, n_i, τ_{Ai}, η, and λ_p depend sharply on the temperature, extrinsic donor impurity concentration, N_d, and the molar fraction, x, in the Hg(1-x)Cd(x)Te material. To assess approximate values for these parameters a match was empirically made to data collected on the detectors by Ed Andrews of ITT[Ref 7]. Additional data have been supplied by Jean Hartley[Ref 8],

4. EXAMPLES OF MODEL CALCULATIONS

Two examples of model calculations are given for detectors to be used in the GOES SN03 satellite. Estimating detector parameters from test data is the first step. Variation of the small-signal responsivity and percent non-linearity, %NL, versus background power and detector temperature is evaluated. Finally, variation of the calibration equation coefficients β_1 and β_2 versus background power and detector temperature is calculated.

4.1 FITTING PARAMETERS

Parameters of the model are derived from detector test data. As described in Appendix A, one of the more critical parameters is the Cd molar fraction, x, in the Hg(1-x)Cd(x)Te alloy. This can be deduced from spectral measurements of the relative responsivity. This is illustrated in Figure 4 and Figure 5.

The 50% relative responsivity wavelength in the cut-off region is a sensitive function of the detector operating temperature. By comparing the observed 50% relative responsivity point, shown as a black dot, to the relative responsivity predicted by the equations for the responsivity given in Appendix A, a value of x can be determined that matches the data.

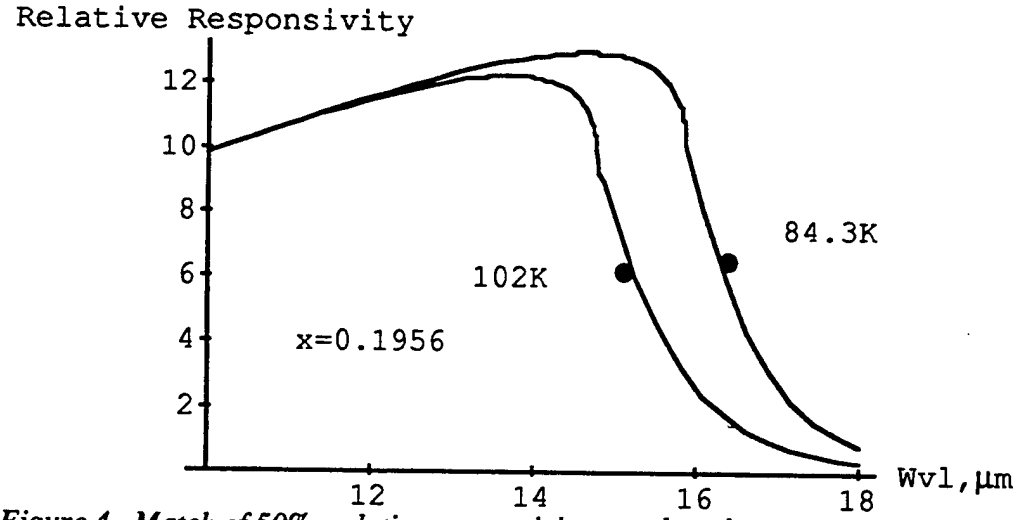

Figure 4. Match of 50% relative responsivity wavelength vs temperature for the Judson LongWave J-033 detector.

For the case of the LIRIS I3-L009 detector the spectral response of the LIRIS I3-L006 has been used. Spectral response data on L009 was not available, but was stated to be virtually identical to L006 [Ref 9].

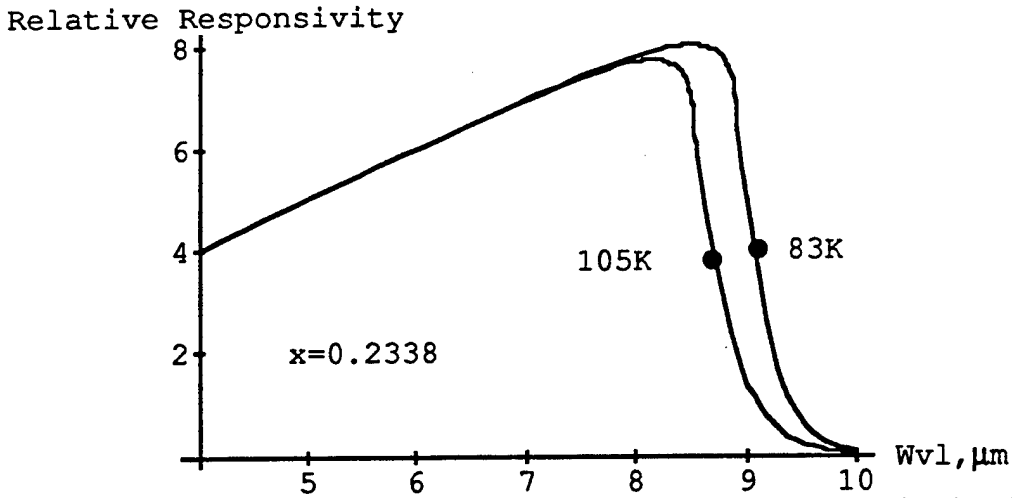

Figure 5. Match of 50% relative responsivity wavelength vs temperature for the LIRIS I3-L006 detector.

It is seen from Figures 4 and 5 that the values of x are 0.1956 and 0.2338, respectively. These two values are for the smallest and largest bandgap material employed in the SN03 instrument, respectively.

The model equations given in Appendix A have a precision that is sensitive to changes in the fourth decimal place of x. However, the absolute accuracy of the equations and the predicted value of x is on the order of $\approx \pm 2\%$.

Matches to other parameters were obtained by comparing the model to measured responsivity and detector resistance versus bias current. The results of this match is given in Table 1. The optical area and bias current assumed is also included in Table 1.

TABLE 1

Detector Parameters

Parameter	I3-L009	J-033
Cd molar fraction, x	0.2338	0.1956
optical area, cm^2	1.07×10^{-4}	3.77×10^{-5}
N_d, $\#/cm^3$	5×10^{14}	3×10^{14}
S, cm/sec	50	50
g_{ss}, mMho	4	7
L_e/L	4	3
R_d, Ohms	≈200(105K)	≈90(102K)
$\Re$[Pb, 0], kV/Watt	≈120(105K)	42(102K)
I_o, mA	1	1

4.2. SMALL-SIGNAL RESPONSIVITY VERSUS BACKGROUND AND TEMPERATURE

Variation of instrument small-signal responsivity with changes in background power and detector temperature is a critical issue[Ref 10]. To evaluate the responsivity from the models it is necessary to estimate the background power and maximum scene power falling on the detectors. Table 2 is a summary of channel characteristics assumed.

TABLE 2

Channel Parameters

Parameter	Imager 3	LW Sounder Ch 7
$\langle\lambda\rangle$	6.75 μm	12 μm
$\Delta\lambda$	0.5 μm	0.7 μm
Max T_{scene}	320K	330K
P_b	12 nWatts	110 nWatts
Max P_s	7 nWatts	16 nWatts

The results of model computations are shown in Figures 6 and 7. Note that in the Figures the responsivity in kV/ Watt is a negative number.

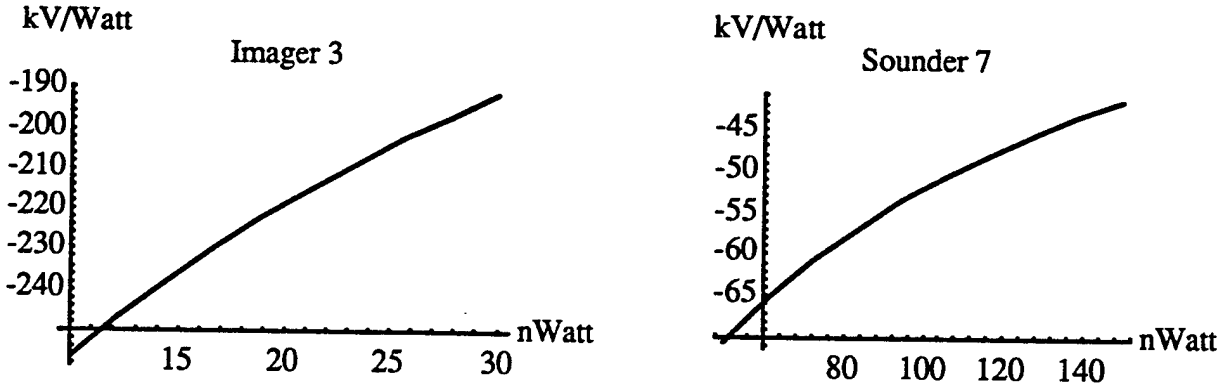

Figure 6. Variation of the small -signal responsivity of Imager 3 and Long Wave Sounder Channel 7 vs background power on the detector. (The temperature of the detectors is 100K.)

It is seen from Figure 6 that both the Imager Channel 3 and the Sounder Channel 7 exhibit a small-signal responsivity that decreases with increasing background power. The decrease is attributable to the decrease in carrier relaxation time,τ, caused by the increasing photo-excited carrier density, n_p, that results from increasing P_b. This effect is indicated by Eqs.(20) and (21).

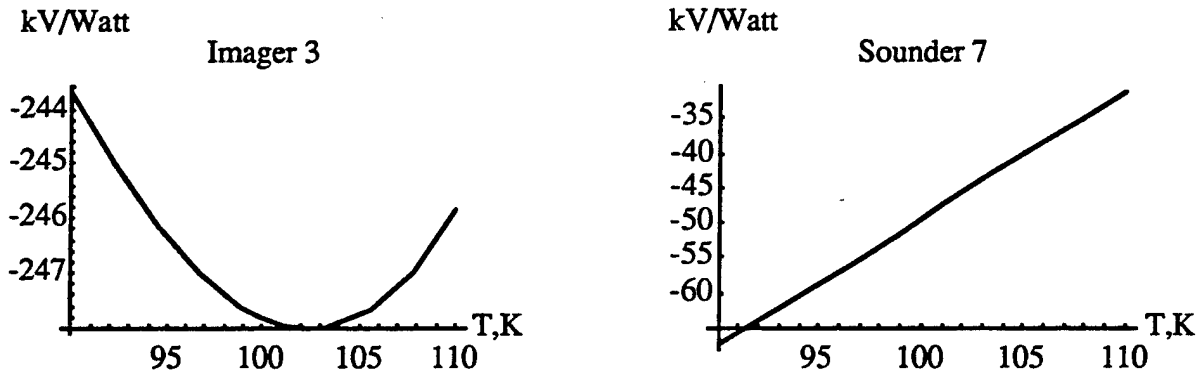

Figure 7. Variation of the small -signal responsivity of Imager 3 and Long Wave Sounder Channel 7 vs detector temperature. (The background power on the detector is 21 nW for the Imager and 110 nW for the Sounder.)

Figure 7 shows a difference between the small-signal responsivity versus detector temperature for the small and large bandgap materials. From Eq.(8) it can be reckoned that the temperature dependence of the small-signal responsivity is influenced by three effects: The electron mobility, μ_e, the carrier relaxation time, τ, and the equilibrium electron density, n_o, which tends to shunt changes in photo-excited conductance.

Electron mobility increases with decreasing temperature, tending to increase the responsivity of both detectors with decreasing temperature. However, the carrier relaxation time and equilibrium electron density dominate the temperature dependence over the operating range shown in Figure 7. These two dominant effects behave differently for the two detectors in the operating temperature range. To heuristically explain this difference in behavior, reference is made to equations in Appendix A.

The Sounder Channel 7 detector has a valence-to-conduction bandgap that is relatively small compared with its thermal energy over the operating temperature range. The small bandgap causes the value of n_i to be large and, in particular, large compared to N_d. This, in turn, causes n_o and p_o to equal, or nearly equal, the intrinsic carrier density, n_i. The intrinsic carrier density, n_i, decreases exponentially with decreasing temperature. This carrier concentration effect is indicated in Eqs. (A5) and (A6).

From Eq.(20) or Eq.(A9b) it can be seen that for $n_o \approx p_o \approx n_i$ the carrier density factors in the numerator and denominator tend to cancel, making the carrier relaxation time proportional to the intrinsic Auger relaxation time, τ_{Ai}. The intrinsic Auger relaxation time, τ_{Ai}, increases with decreasing temperature as indicated in Eq.(A9a).

The increase of the responsivity of the Sounder Channel 7 detector with decreasing temperature results from the decrease of n_o(less shunt conductance) and the increase of τ_{Ai}(longer carrier lifetime) with decreasing temperature.

The Imager 3 detector has a bandgap that is relatively large compared with its thermal energy over the operating temperature range. This causes the value of n_i to be relatively small and on the order of N_d over the operating temperature range. This in turn, causes n_o to equal, or nearly equal, the detector's donor impurity density, N_d, and the value of p_o to be small. This carrier concentration effect also results from Eqs. (A5) and (A6). From Eq.(20) or Eq.(A9b) it

can be seen that for $p_o << n_o \approx N_d$ the carrier relaxation time is proportional to the product, $n_i^2 \tau_{Ai}$. The product $n_i^2 \tau_{Ai}$, decreases with decreasing temperature due to the strong, exponential dependence of n_i on temperature as given by the b_i factor in Eq.(A5).

At higher operating temperatures, decreasing the temperature increases the Imager 3 detector responsivity. This is because the mobility increases and because the detector is in a carrier density regime similar to that of the Sounder Channel 7 detector described above.

Upon decreasing temperature, a temperature is reached for which $n_o \approx N_d$. At this temperature the carrier relaxation time, τ, becomes proportional to the product $n_i^2 \tau_{Ai}$. The small-signal responsivity will then decrease with decreasing temperature due to the decrease of carrier lifetime The result is the weak maximum in the Imager 3 small-signal responsivity exhibited in Figure 7.

The model demonstrates that the temperature dependence of the small-signal responsivity is significantly influenced by the doping level, N_d, the Cd molar fraction, x, which determines the HgCdTe alloy bandgap, and by the operating temperature range.

4.3 PERCENT NON-LINEARITY

An estimate of the percent non-linearity is calculated for the two detectors. Results of the calculations are shown in Figure 8. Note that the value of %NL shown is negative. The percent non-linearity for a fixed background flux increases with increasing signal, or scene, power.

The percent non-linearity reaches ≈4-6% at high scene flux levels. Based on the inference drawn from Eq.(1) and from Figure 1, this is a significant non-linearity at longer wavelengths with regard to calibration. Thus, the detector and preamplifier circuit non-linearity is an important issue to the GOES instrument calibration.

Comparing Eq.(27) with Eq.(13) indicates that a quadratic or higher-order variation in %NL versus P_S would result from a cubic or higher-order dependence of the responsivity on P_S. Figure 8 shows that the %NL is linear with respect to P_S, or nearly so, and does not exhibit a significant higher-order dependence on P_S. Thus, the responsivity, $\Re(P_b, P_S)$, is suitably represented by a quadratic function in P_S for a given background flux level.

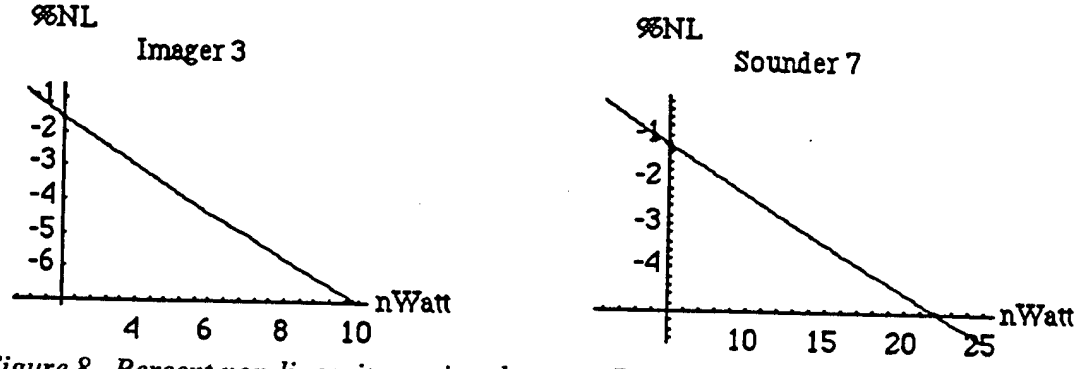

Figure 8. Percent non-linearity vs signal power, P_S. (Operating temperature is 100K with background power of 16nW and 110nW on I3 and the LW Sounder Ch 7, respectively.)

The percent non-linearity associated with the detector, $\%NL_\tau$, given in Eq.(29) was evaluated. It was found that approximately 70% of the non-linearity was due to the dependence of the carrier relaxation time on the photo-excited carrier density, n_p, as given by Eq.(20). I.e., for the SN03 Imager 3 and Sounder Channel 7 the detector non-linearity, rather than the circuit non-linearity, was found to cause ≈70% of the overall non-linearity.

4.4 CALIBRATION EQUATION COEFFICIENTS

The model calibration equation is a polynomial in Δcounts as described in Section 2.2. For a quadratic fit, the coefficients of the Δcount terms, b_1 and b_2, are proportional to parameters β_1 and β_2, respectively, as given by Eq(18).

In-orbit correction of calibration coefficients relies on two data points collected for each channel. The data points are to be used to adjust offset term(not in the model) and the linear term, β_1. The quadratic term, β_2, is to be adjusted using telemetered temperature data from the satellite. Predicted in-orbit variation of β_1 and β_2 due to detector and detector circuit responsivity is a goal of the modeling effort.

Figures 9 and 10 show the variation of β_1 versus background power and detector temperature. Note the values of β are negative.

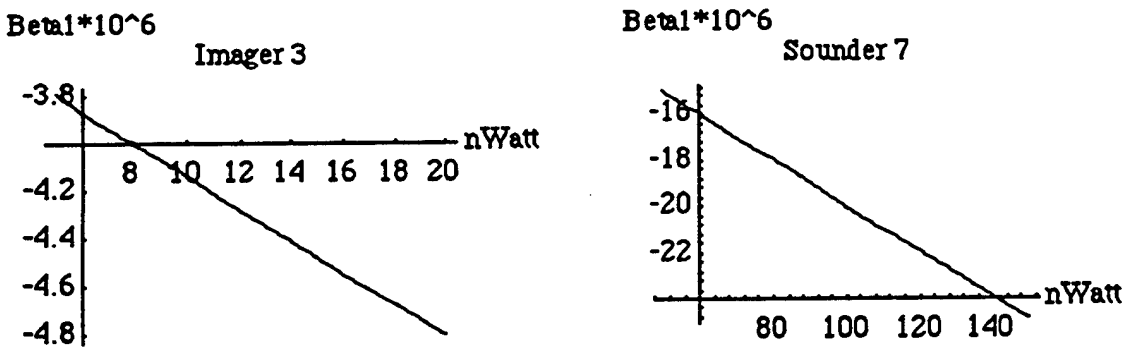

Figure 9. Variation of β1 for Imager 3 and Long Wave Sounder Channel 7 vs background power. (The temperature of the detectors is 100K.)

Figure 9 shows that for both Imager 3 and Long Wave Sounder Channel 7 β_1 increases in magnitude with increasing background power. This is consistent with the dependence of the small-signal responsivity versus background power shown in Figure 6: The responsivity decreases in magnitude, causing the calibrated estimate of impinging radiance given by the calibration equation to increase for a given value of Δcounts.

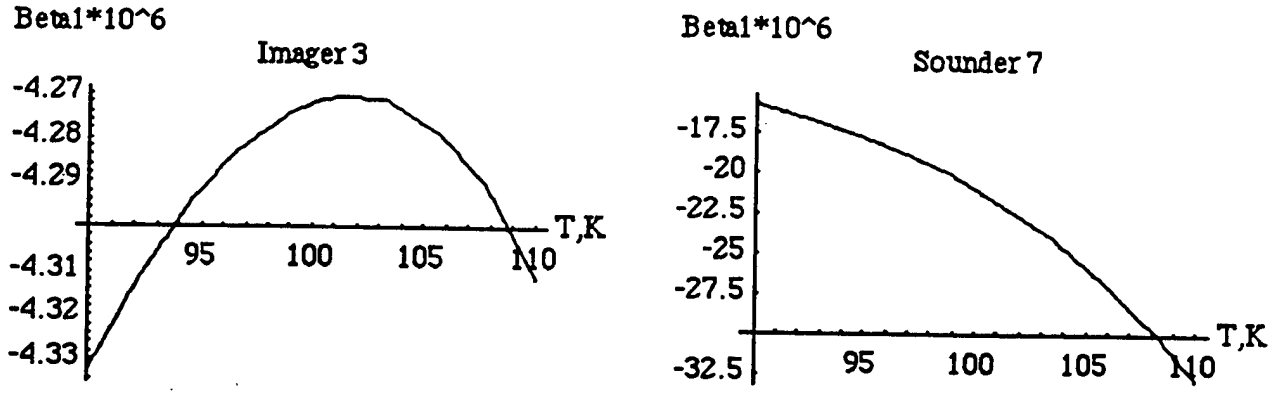

Figure 10. Variation of β_1 of Imager 3 and Long Wave Sounder Channel 7 vs detector temperature. (The background power on the detector is 21 nW for the Imager and 110 nW for the Sounder.)

The variation of β_1 to changes in detector temperature for Imager 3 and Sounder Channel 7 shown in Figure 10 reflect the comparative small-signal reponsivity versus detector temperature shown in Figure 7: Imager 3 exhibits a local minimum in β_1. For Sounder Channel 7 the magnitude of β_1 increases with increasing temperature and is more sensitive to temperature than the β_1 coefficient of Imager 3.

Figures 11 and 12 show the effects of background power and temperature predicted by the model on the β_2 coefficient. This coefficient is to be corrected using in-orbit calibration measurements and chamber test data as described in Section 1.1.

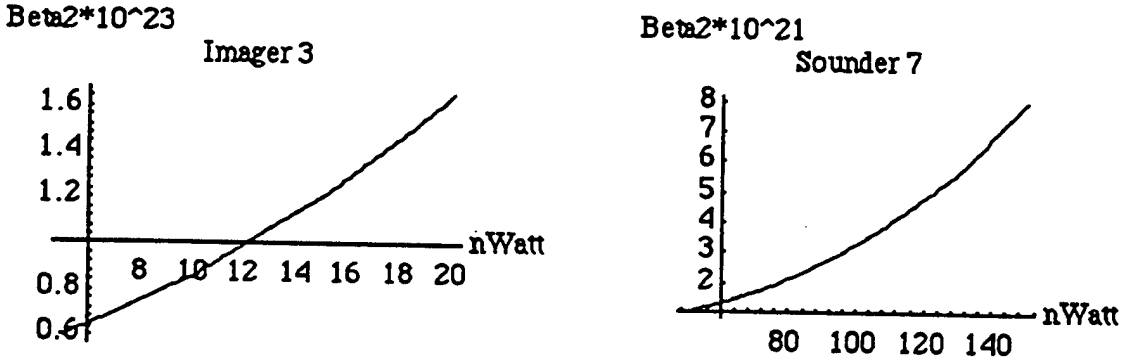

Figure 11. Variation of β_2 of Imager 3 and Long Wave Sounder Channel 7 versus background power. (The temperature of the detectors is 100K.)

Figure 11 indicates that the β_2 coefficient increases with increasing background power for both Imager 3 and Sounder Channel 7. The β_2 coefficient of the Sounder Channel 7 is significantly more sensitive to background power than the Imager 3 channel.

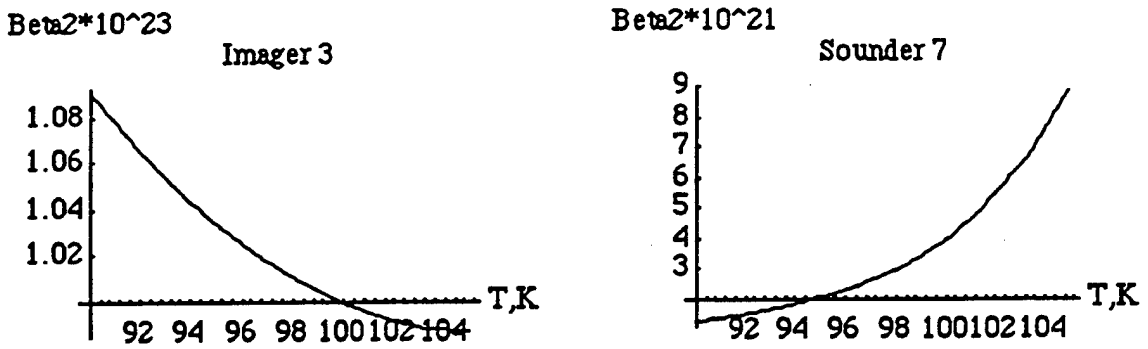

Figure 12. Variation of β_2 of Imager 3 and Long Wave Sounder Channel 7 vs detector temperature. (The background power on the detector is 21 nW for the Imager and 110 nW for the Sounder.)

Figure 12 indicates that the variation of β_2 with detector temperature decreases with increasing temperature over the operating range while the β_2 coefficient of the Sounder Channel 7 increases. The sensitivity of the Sounder Channel 7 coefficient to temperature is significantly greater than Imager 3.

Figures 11 and 12 indicate that the variation of β_2 with background power(optics baffle temperature) and detector temperature depends in an approximately quadratic manner on these parameters. Interpolation between pre-orbit chamber test data points and in-orbit measurements will be required to correct β_2. The model indicates that a quadratic interpolation scheme should be satisfactory.

5. SUMMARY

A small, few percent($\leq$ 5%) non-linearity in responsivity, if not acounted for in instrument calibration, could significantly affect the accuracy of the products provided by the GOES satellite, especially at longer wavelengths. Determining response non-linearity is a driver in the amount of required pre-launch instrument chamber testing. Response non-linearity is due to the HgCdTe detector and preamplifier circuitry employed by GOES instruments.

Analysis of HgCdTe detector and preamplifier response non-linearity was undertaken based on detector physics reported in the literature. Although the analysis did not consider flux-dependent non-linearity resulting from sweepout effects due diffusion and electric bias fields, it should apply to GOES instruments employing detectors biased up to $\approx$2.0-3.0 mA.

The analysis also related instrument responsivity and the OGE calibration equation. No rationale was uncovered for a constant offset term in the OGE calibration equation, although such a term is employed in practice based on pre-launch chamber tests. Further pursuit of the cause of the offset term is recommended.

A computer code model of the GOES instrument responsivity was developed. The objective was to develop a model that could be utilized to expedite pre-launch calibration of GOES satellite instruments and to provide confidence in GOES in-orbit calibration procedures.

The model was used to examine the responsivity of two SN03 instrument detectors. Results indicate that the percent non-linearity of the response of these detectors and their pre-amplifier circuits can reach 4-6%, which is significant to calibration. Both the detector and the pre-amplifier circuit contribute, and contribute additively, to the percent non-linearity. The detector contribution was dominant, being as much as $\approx$70%.

It was found that an OGE calibration equation of quadratic order suitably describes the non-linearity due to HgCdTe detectors and detector preamplifer circuitry. The calibration equation's quadratic coefficient was found, itself, to have up to a quadratic dependence on background power and detector temperature, indicating that a quadratic interpolation technique would be suitable for its in-orbit adjustment to variation in these parameters.

6. REFERENCES

1. Data provided by Michael P. Weinreb, Physics Branch, NOAA/NESDIS, Camp Springs, Maryland.

2. M.P. Weinreb, G. Hamilton, S. Brown, R.J. Koczor, "Nonlinearity Corrections in Calibration of Advanced Very High Resolution Radiometer Infrared Channels," *J. of Geophysical Research*, Vol 95, No. C5, pp 7381-7388, 15 May 1990.

3. M.P. Weinreb, Private Communication.

4. D. Cousins, R. Heinrichs, E. Wack, Private Communication, MIT Lincoln Laboratory, Lexington, MA, 12 November 1992.

5. R.B. Schoolar, W.E. Bicknell, D.L. Spears, "HgCdTe LWIR Photoconductor Technology Review and Performance Projections of GOES Imager-4, Imager-5, and LW Sounder," Aerospace Corporations Report ATR-92 (2826)-1, July 1992.

6. M.B. Reine, Loral Infrared Imaging Systems (LIRIS), Lexington, MA, Private Communication.

7. J.E. Andrews, D. Pierre, "GOES SNO3 Imager/Sounder HgCdTe Detector Data Summaries," preliminary release, ITT, Ft. Wayne, IN, 24 June 1992.

8. Data provided by J. Hartley, Loral Infrared Imaging Systems (LIRIS), on the responsivity and noise vs. bias current for GOES SNO3 detectors, Lexington, MA, 24 June 1992.

9. E. Andrews, ITT, Ft. Wayne, IN, Private Communication.

10. K. Mason, Loral Infrared Imaging Systems (LIRIS), Lexington, MA, Private Communication, July 1992.

APPENDIX A

HgCdTe DETECTOR MODEL

This appendix summarizes the detector physics and computational procedures used for calculating GOES detector and detector-circuit responsivity. It duplicates some of the discussion in the main body of the report. It is intended as a bridge between the main body of the report and the actual code employed given in Appendix B.

1 ENERGY GAP, QUANTUM EFFICIENCY, AND Cd MOLAR FRACTION

The bandgap energy, E_g, vs the temperature, T, in degrees K and molar fraction of Cd, x, is taken from the work of Hansen,Schmit, and Casselman[Ref 1].

$$E_g = (-0.302 + 0.000535\,T\,(1 - 2\,x) + 1.93\,x - 0.81\,x^2 + 0.832\,x^3), \text{eV} \qquad \text{(A1)}$$

The gap energy equals the energy of a photon at a "cut-off" wavelength, λ_{co} given by

$$\lambda_{co} = \frac{1.2399}{E_g}, \ \mu\text{m} \qquad \text{(A2)}$$

The quantum efficiency, η, gives the ratio of photo-excited carriers to the photon flux intensity impinging on the detector. The expression used is taken from the report by Schoolar, Bicknell, and Spears and references cited therein[Ref 2].

$$\eta = (1-R)\frac{1 - \text{Exp}[-2\alpha H]}{1 - R\,\text{Exp}[-2\alpha H]} \qquad \text{(A3)}$$

where

α = absorption coefficient, cm^{-1}
H = detector height = 0.0008 cm
R = front surface reflection coefficient.

The value for the absorption coefficient at a wavelength for which the photon energy equals E_p is taken from work reported by Schoolar in Reference 2.

$$\alpha = \alpha_o\left(1+15\sqrt{E_p - E_g}\right), \text{cm}^{-1} \qquad E_p \geq E_g \qquad \text{(A4a)}$$

$$\alpha = \text{Exp}\left[\frac{2.38(E_p-E_g)}{kT}\right], \text{cm}^{-1} \qquad E_p < E_g \qquad \text{(A4b)}$$

where:

$\alpha_o = 1770\sqrt{Eg}$, cm^{-1}
T in degree K
E_g and E_p in eV
k = Boltzman's constant = 1.38066×10^{-23} Joule/degree K
1 Joule = $1/(1.60218 \times 10^{-19})$ eV
$k = 8.617 \times 10^{-5}$ eV/degree K.

Quantum efficiency determines the wavelength dependence of the responsivity of the detector. Using relative spectral responsivity data collected by ITT and the above equations, an estimate of x has been obtained for two GOES-NEXT SN03 detectors. The estimate was made by graphically fitting relative responsivities predicted by the equations at two operating temperatures to the measured 50% relative responsivity points in the cut-off wavelength region. The value of R = 0 was used for the estimated match. The estimates are listed in Table A1. Values of x used in Reference 2 in describing expected GOES-NEXT detector performance are also listed.

TABLE A1

Estimated values of x

Detector	Temperatures(K)	Estimated x	[Ref 2]
MW-L002	102, 80.9	0.2120	-----
LW-J033	102, 84.3	0.1956	0.19I3
L006	105, 83	0.2338	-----
I4-L002	105, 84	0.2080	0.209
I5-J019	105, 82	0.2035	0.203

The 50% relative response points agree at the two temperatures to about ± 2% in wavelength. Although indicated to 4 decimal places, the accuracy of the estimated value of x is no better than ± 5%.

2 INTRINSIC AND EQUILIBRIUM CARRIER CONCENTRATION

Intrinsic carrier concentration, n_i, is taken from the work of Hansen and Schmit[Ref 3].

$$a_i = 5.585 + 0.001753\,T - 3.82(x) - 0.001364\,(xT)$$

$$b_i = 10^{14}\,\frac{E_g^{0.75}\;T^{1.5}}{\mathrm{Exp}\left[5802.84\,\frac{E_g}{T}\right]}$$

$$n_i = a_i b_i, \quad \frac{\#}{cm^3} \qquad \text{(A5)}$$

Equilibrium density of electrons, n_o, and holes, p_o, in the conduction and valence bands in the case of a material donor impurity density, N_d, is given by

$$n_o = +\frac{N_d}{2} + \sqrt{\left(\frac{N_d}{2}\right)^2 + (n_i)^2}\ , \quad \frac{\#}{cm^3} \tag{A6a}$$

$$p_o = -\frac{N_d}{2} + \sqrt{\left(\frac{N_d}{2}\right)^2 + (n_i)^2}\ , \quad \frac{\#}{cm^3} \tag{A6b}$$

as described in Blakemore[Ref 4]. The values of n_o and p_o are determined by simultaneously solving the equation for charge neutrality and the equation for carrier equilibrium in a non-degenerate semiconductor:

$$(n_i)^2 = n_o p_o \,. \tag{A7}$$

3 ELECTRON AND HOLE MOBILITY

Values of electron and hole mobilities are taken from work reported by Schoolar in Reference 2.

$$\mu_e = \frac{1}{2.5\ 10^{-7}\ T^{1.5}\ x2\ + \frac{0.0313\ x4}{T^{1.5}}}\ , \frac{cm2}{Volt\text{-}Sec} \tag{A8a}$$

$$\mu_h = \frac{1}{\frac{5.26\ 10^{-7}\ T^{1.5}}{x} + \frac{4000\ x7}{T^{1.5}}}\ , \frac{cm2}{Volt\text{-}Sec} \tag{A8b}$$

4 CARRIER RECOMBINATION LIFETIME

The effective carrier relaxation time,τ, is determined by both Auger recombination and surface recombination processes.

4.1 AUGER RECOMBINATION

The dominant mechanism in carrier recombination is the Auger process[Ref 5]. The intrinsic population(n_o=p_o=n_i) Auger relaxation time, τ_{Ai}, is given by

$$\tau_{Ai} = \frac{3.75048\ 10^{-7} Exp\left[\frac{11605 E_g}{T}\right]\sqrt{E_g}}{T^{1.5}}, Sec \tag{A9a}$$

where the dependence of τ_{Ai} on the temperature, bandgap energy, and electron effective mass is taken from Reference 5. The effective mass of a conduction band electron is taken to be proportional to the bandgap energy and a scaling coefficient has been chosen to give agreement with data in Reference 5 using the above Eqs.(A1) and (A5) for n_i[x,T], and E_g[x,T][Ref 6].

For the non-intrinsic case where n_p is the electron carrier concentration induced by photon flux the Auger relaxation time, τ_A, is given by

$$\tau_A = \frac{2(n_i)^2\tau_{Ai}}{(n_o+n_p)(n_o+p_o+n_p)} = \frac{2n_op_o\tau_{Ai}}{(n_o+n_p)(n_o+p_o+n_p)}, \text{Sec} \qquad \text{(A9b)}$$

4.2 SURFACE RECOMBINATION

As described in Reference 2 and references cited therein, surface recombination alters carrier recombination lifetime. The effect of surface recombination depends on the ambipolar diffusion constant, D_a, given by[Ref 7]

$$D_a = 8.61710^{-5}T\frac{(n_o+p_o+2n_p)\mu_e\mu_h}{(n_o+n_p)\mu_e+(p_o+n_p)\mu_h}, \frac{cm}{Sec} \qquad \text{(A10)}$$

where

$$\frac{kT}{q} = 8.617\ 10^{-5}\,T, \frac{Joule}{Coulomb}, \text{T in degrees K.}$$

A parameter that depends on D_a is the ambipolar drift length, L_a, given for a carrier recombination time, τ_A, by

$$L_a = \sqrt{D_a\tau_A}, \text{ cm} \qquad \text{(A11)}$$

The effect of surface recombination on the effective carrier relaxation time,τ, is given as

$$\tau = A_1\tau_A \qquad \text{(A12)}$$

where

$$A_1 = \frac{\text{Sinh}\left[\frac{H}{L_a}\right] + \frac{S\tau_A}{L_a}\left(\text{Cosh}\left[\frac{H}{L_a}\right] - 1\right)}{\left\{1+\left(\frac{S\tau_A}{L_a}\right)^2\right\}\text{Sinh}\left[\frac{H}{L_a}\right] + 2\frac{S\tau_A}{L_a}\text{Cosh}\left[\frac{H}{L_a}\right]}. \qquad \text{(A13)}$$

5 FLUX DEPENDENT CARRIER LIFETIME

The flux dependence of the carrier lifetime, τ, is the principal cause of photo-conductor response non-linearity.

5.1 FLUX DEPENDENT AUGER LIFETIME

As indicated by Eq.(A9b) and as experimentally determined by Bartoli et al, the Auger lifetime, τ_A, and thus the effective carrier lifetime, τ, depends on the carrier concentration generated by photon flux, n_p[Ref 8]. For an incident photon flux Q_p, #/cm^2-Sec, the value of n_p is given by

$$n_p = \frac{\eta \tau Q_p}{H}, \ \frac{\#}{cm^3} \tag{A14}$$

Combining Eq.(A9b) with Eq.(A12) and substituting the result into Equation (A14) leads to the following cubic equation for n_p:

$$\left(\frac{n_p}{n_i}\right)^3 + \frac{2n_o+p_o}{n_i}\left(\frac{n_p}{n_i}\right)^2 + \frac{n_o+p_o}{p_o}\left(\frac{n_p}{n_i}\right) = \frac{2\eta\tau^*_{Ai}Q_p}{n_i H} \tag{A15}$$

where

$$\tau^*_{Ai} \equiv \tau_{Ai} A_1 .$$

The solution of Eq.(A15) satisfies both Equation (A9b) and (A14). The effect of surface recombination introduces two computational complications: First, equation (A15) must be solved to evaluate τ_A from Eq.(A9b). But, τ_A must be known in order to evaluate L_a from Eq.(A11) and A_1 from Eq.(A13). A second complication is that L_a depends on D_a which, as indicated in Eq.(A10), depends on n_p.

A solution to this problem was accomplished by Marion Reine of (now) LIRIS in 1979 for ATMOS detectors operated at 77K[Ref 9]. Marion used a different approach for accounting for the surface recombination effect, but incorporated its flux dependence.

5.2 ITERATIVE SOLUTION FOR τ AND n_p

The following is the iterative technique used for self-consistently solving Eqs. (A9b), (A10), (A11), (13), and (A15):

Let $n_p[j]$ be the jth estimate of n_p.

(i) Given that $\{n_o, p_o, \tau_{Ai}\}$ are calculated for a given $\{N_d, x, T\}$, an estimate of τ_A, $\tau_A[j]$, may be obtained from Eq.(A9b) using $n_p[j]$.

(ii) Also using $n_p[j]$, Eq.(A10) may be evaluated to give an estimate of D_a, $D_a[j]$. Then, using $D_a[j]$ and $\tau_A[j]$, Eq(A11) may be solved for an estimate of L_a, $L_a[j]$.

(iii) Using $L_a[j]$ and $\tau_A[j]$, Eq(A13) may be solved for an estimate of A_1, $A_1[j]$.

(iv) The value of $A_1[j]$ may then be used to compute

$$\tau^*_{Ai}[j] \equiv \tau_{Ai} A_1[j].$$

(v) Letting $N_p\{n_o, p_o, Q_p, \tau^*_{Ai}[j]\}$ denote the single positive n_p root of Eq.(A15), the (j+1)th estimate of n_p is given by

$$n_p[j+1] = N_p\{n_o, p_o, Q_p, \tau^*_{Ai}[j]\}$$

and the iteration is repeated.

The goal of the iteration is to accurately estimate τ for a given Q_p and to accordingly assess n_p. Upon the iterative procedure converging, the iteration is ended when

$$\left|\frac{\tau[j+1]}{\tau[j]} - 1\right| \approx 1\%.$$

The initial value of n_p, $n_p[0]$ is taken from Eq (A14) with $\tau[0] = \tau_{Ai}$. A solution is described by the order of the iteration undertaken. Results are reported using 10th or higher order solutions.

6 DETECTOR REPONSIVITY

Determining the responsivity of the GOES detectors requires separating Q_p into two components,

$$Q_p = Q_b + Q_s$$

where Q_b is a background flux that is assumed constant on the detector both between and throughout measurements and Q_s is the signal flux incident on the detector during a look at an earth scene. Thus, from Eq.(A14) the photo-excited carrier concentration, n_p, is also composed of two components, n_b and n_s from the background and the signal flux, respectively.

The relation between incident flux, Q_p, and the incident power, P_p, in watts at the cutoff wavelength, λ_{co}, is

$$Q_p = \frac{\lambda_{co} P_p}{hc\ WL'}\ \frac{\#}{cm^2\text{-Sec}} \qquad \text{(A16)}$$

where

h = Planck's Constant = 6.63×10^{-34} Joule-Sec

c = speed of light = $3 \times 10^{14}\ \frac{\mu m}{Sec}$

and where W is the width and L the optical sensitive length of the detector. Thus, the power incident on the detector is composed of two components, P_b and P_s, from the background and the signal, respectively.

The responsivity is evaluated at the peak response wavelength which is assumed here to be λ_{co}. The responsivity is evaluated in two steps:

First, a voltage is computed for $n_p = n_b$. This voltage will depend on the detector resistance, $R_d[n_p]$ for an incident flux. $R_d[n_p]$ is given by:

$$R_d[n_p] = \frac{1}{q\left\{\frac{2N_{ss}\mu_{ss}}{H} + \mu_e(n_o + n_p)\right\}\frac{HW}{L_e}}, \text{ Ohms} \qquad \text{(A17)}$$

where

$q = 1.60218 \times 10^{-19}$ Coulombs
H = detector width, approximately = 0.8×10^{-3} cm
W = detector width
L = detector photo-responsive length ≈W ≈ (5.0-7.5) 10^{-3} cm
W•L = photo-responsive area
L_e = detector electrical length, ≈(2-4)L
$(N_{ss}\ \mu_{ss})$ = Surface State (population-density mobility) product≈(2-5)10^{16}, #/Volt-Sec

The value of the $(N_{ss}\ \mu_{ss})$ product depends on propietary fabrication processes and the estimate given is only an edjucated guess. The estimated values give a shunt conductance value, g_{ss}, where

$$g_{ss} = 2\ q(N_{ss}\ \mu_{ss})W/L_e,$$

of approximately (4-7) mMho for SNO3 detectors. Values are estimated from detector resistance vs bias and temperature data.

Given $R_d[n_p]$ the detector preamplifier voltage,$V[P_p]$, is determined by the bias current, I_o, the bias voltage, V_o, and the bridge bias resistor value, R_b.

$$V[P_p] = I_o \frac{R_d[P_p]}{R_b + R_d[P_p]}, \text{ Volts} \qquad \text{(A18)}$$

$$I_o = \frac{V_o}{R_b}, \text{ Amps and } V_o = 10 \text{ Volts.}$$

The second step is the evaluation of $V[P_b + P_s]$, which follows from Eq.(18) with $P_p = (P_b + P_s)$. The preamplifier earth scene signal voltage, $\Delta V[P_s]$, is then evaluated as the difference between $V[P_b + P_s]$ and $V[P_b]$.

$$\Delta V[P_s] = V[P_b + P_s] - V[P_b].(19) \qquad \text{(A19)}$$

Equation (A19) gives the basic expression for the investigated GOES SN03 responsivity non-linearity.

7 DETECTOR SMALL-SIGNAL RESPONSIVITY AND PC GAIN

Two parameters that are of interest in assessing detector performance are the small-signal responsivity and the photo-conductive(PC) gain.

A small-signal voltage responsivity, $\Re[P_b,0]$, is taken to be

$$\Re[P_b,0] = \underset{P_s \to 0}{\text{Limit}} \frac{\Delta V}{P_s} = \frac{dV[P_p]}{dP_p} = \frac{dV[n_p]}{dn_p}\frac{dn_p}{dQ_p}\frac{dQ_p}{dP_p} = \frac{\eta\lambda_{co}}{hcHWL}\frac{dV[n_p]}{dn_p}\frac{d(Q_p\tau[Q_p])}{dQ_p}\Bigg|_{\substack{Q_p=Q_b \\ n_p=n_b}} \quad \text{(A20)}$$

Equation (A20) indicates that the derivative of $\tau[Q_p]$ evaluated at $Q_p = Q_b$ plays a role in the small-signal responsivity, which is born out by modeling results. Taking $R_b >> R_d[P_b]$ in Eq.(A18), the small-signal responsivity is given by Eq.(A20) to be

$$\Re[P_b,0] \cong -0.8\,\eta\, I_o\, \mu_e\, \tau_{eff}[P_b]\, \frac{\lambda_{co}}{LL_e}(R_d[P_b])^2,\ \frac{\text{Volt}}{\text{Watt}} \quad \text{(A21)}$$

where

$$\tau_{eff}[Q_b] = \tau[Q_b] + Q_b \frac{d\tau[Q_p]}{dQ_p}\Bigg|_{Q_p=Q_b}.$$

In the computer code, the small signal gain for a given P_b is evaluated by determining the responsivity for a signal power that is 0.00000001% of the background power. This small signal flux responsivity is taken to be the responsivity the detector approaches as $P_S \to 0$.

The photo-conductive gain, G_{pc}, is defined as the ratio of the mean free path of a photo-excited carrier to the photo-electrically sensitive length(L) of the detector. When a carrier transits the detector and is swept into a collecting contact, charge conservation requires that the opposite contact emit a carrier. The idea is that a single photo-electrically excited carrier may effectively transit the detector several times. The gain gives the number of transits for $L=L_e$.

The mean free path of the carrier is just its effective lifetime, τ_{eff}, multiplied by its mean velocity, $\mu_e E$, where E is the electric field due to the bias voltage. In this case the voltage across the detector is given by the product $(I_o R_d)$ leading to

$$G_{pc} = \frac{1}{L}\left(\frac{\mu_e I_o R_d[P_b]}{L_e}\tau_{eff}[P_b]\right)$$

So, considering Eq.(A21)

$$\Re[P_b,0] \cong -0.8\lambda_{co}\,\eta\, G_{pc}\, R_d,\ \frac{\text{Volt}}{\text{Watt}}.$$

Measurement of the responsivity and the detector resistance, and hence the inference of the $(\eta\, G_{pc})$ product, is often undertaken to characterize detectors.

APPENDIX A REFERENCES

1. G. L. Hansen, J.K. Schmit, T.N. Casselman, *J. Appl. Phys.*, 53 (10), 1982, pp. 7099-7101.

2. R.B. Schoolar, W.E. Bicknell, D.L. Spears, "HgCdTe LWIR Photoconductor Technology Review and Performance Projections of GOES Imager-4, Imager-5, and LW Sounder." Aerospace Corporation Report ATR-92 (2826)-1, July 1992.

3. G.L. Hansen, J.L. Schmit, *J. Appl. Phys.*, 54 (3), 1983, pp. 1639-1640.

4. J.S. Blakemore, *Semiconductor Statistics*, Dover Publications, New York, 1987, pp. 106-113.

5. M.A. Kinch, M.J. Brau., A. Simmons, *J. Appl. Phys.*, 44 (4), 1973, pp. 2649-2663.

6. D. Spears, Private Communication.

7. J.P. McKelvey, *Solid State and Semiconductor Physics*, Kriegger, Malabar, FL, 1984, p. 328.

8. F. Bartoli, R. Allen, L. Esterwitz, M. Kruer, *J. Appl. Phys.*, 45 (5), 1974, pp. 2150-2154.

9. M. Reine, "Non-Linear Response of 8-10 micrometer (Hg, Cd)Te Photoconductor to Large Signal Photon Flux Levels," Memorandum, Honeywell, Lexington, MA, 1979.

APPENDIX B

COMPUTER CODE

Calculations employed the code listed in this Appendix. The code is written for execution in Mathematica and is similar, but not identitical to, C language. Mathematica can convert this code to C or to Fortran.

It is suggested that anyone wishing to calculate detector performance compose their own code. This listing is given to serve as a guide to one way it can be done.

The code is comprised of two functions: f[] and perfP[]. The functions take as input the variables_ listed within the brackets[]. Variables have to start with a lower case character and Greek symbols and subscripts are not supported by Mathematica code. Thus, N_d->nD, S->s, Q_p->qp, e_g->eg, λ->wvl, etc.

The first function, f[], takes basic the parameters [x, T, N_d, S, Q_p] and solves for the equilibrium carrier population density, n_p and the carrier lifetime. It does so using a Do-loop that cycles "kay" times. In practice I have found kay=10 gives satisfactory results. The function returns these values and other intermediate results that are useful in calculating the responsivity of the detector.

```
f[x_,t_,nD_,s_,qp_,kay_]:=

                    (*Define variables used within the function*)
Module[{eg,wvl,ai,bi,ni,no,po,tAi,muE,muH,a,b,np,tAug,do,doN,doD,la,xa,xb,aA,tAiE,c,root},

                    (*Calculate fixed quantities*)
eg=-0.302+1.93*x-0.810*(x^2)+0.832*(x^3)+5.35*(10^-4)*t*(1-2*x);
wvl=1.2399/eg;

ai=5.585-3.82*x+(1.753*10^-3)*t-(1.364*10^-3)*x*t;
bi=(10^14)*(eg^0.75)*(t^1.5)*Exp[-eg/(2*(8.617*10^-5)*t)];
ni=ai*bi;

no=(nD/2)+Sqrt[((nD/2)^2)+ni^2];
po=-(nD/2)+Sqrt[((nD/2)^2)+ni^2];

tAi=(3*10^-13)*(((eg/((8.617*10^-5)*t))^1.5)/eg)*Exp[eg/((8.617*10^-5)*t)];

muE=(2.5*(10^-7)*(x^2)*(t^1.5)+3.13*(10^-2)*(x^4)*(t^-1.5))^-1;
muH=(5.26*(10^-7)*(x^-1)*(t^1.5)+4.0*(10^3)*(x^7)*(t^-1.5))^-1;
        (*All fixed quantities are calculated->Next enter into iterative calculation*)

                    (*Do-loop statement*)
Do[
a=N[(2*no+po)/ni];
b=N[1+(no/ni)^2];
np[0]= ((2*tAi*(ni^2))/(no*(no+po)))*(qp)/0.0008;
aA[0]=1;
tAug=2*tAi*aA[k-1]*(ni^2)*(((no+po+np[k-1])*(no+np[k-1]))^-1);
```

```
doN=8.617*(10^-5)*t*(no+po+2*(np[k-1]))*muH*muE;
doD=((no+np[k-1])*muE)+((po+np[k-1])*muH);
do=doN/doD;
la=(do*tAug)^0.5;
xa=0.0008/la;
xb=s*tAug/la;

aA[k]=N[(Sinh[xa]+xb*(Cosh[xa]-1))*(((1+(xb^2))*Sinh[xa]+2*xb*Cosh[xa])^-1)];

tAiE=tAi*aA[k];
c=N[(2*tAiE/(0.0008*ni))*qp];
root={ToRules[NRoots[y^3+a*y^2+b*y-c==0,y]]};
np[k]=ni*(y/.root[[3]]),{k,1,kay}];
                              (*Finish of Do-loop statement*)

tAugO=2*tAi*aA[kay]*(ni^2)*(((no+po+np[kay])*(no+np[kay]))^-1);

                          (*Return list of results to 12 place precision*)
N[{tAugO,np[kay],muE,wvl,no,ni,tAugO*qp/0.0008},12]
]
```

The function perfP[] takes as an argument the parameters [x, T, N_d, S, I_o, g_{ss}(surface state shunt conductance in Mhos), Adet(area of det in cm^2), r(ratio of L_e/L), P_b, P_s] and calculates the voltage generated by the detector for incident flux due to P_b, $P_b(1+10^{-10})$, and P_b+P_s. From these results the small and large signal responsivites are calculated. The percent change from small to large signal responsivity is assessed. Also, the percent change in the effective carrier lifetime for small and large signal response is evaluated. The function returns a list of several parameters that are of interest to the detector and detector preamplifier operation.

```
perfP[x_,t_,nD_,s_,io_,gss_,aDet_,r_,pb_,ps_,kay_]:=

                          (*Define variables used within the function*)
Module[{b1,b2,rB,fb,rDb,rDbs,rDbSS,vb,fbs,vbs,sig,resp,respNL,percentNL,percenttau,qbSS,vb
SS,respSS,qb,qs,wvl,eg},

                          (*Calculate fixed quantities*)
rB=(10.0)/io;

eg=-0.302+1.93*x-0.810*(x^2)+0.832*(x^3)+5.35*(10^-4)*t*(1-2*x);
wvl=1.2399/eg;

qb=pb*wvl/(aDet*2*(10^-19));
qs=ps*wvl/(aDet*2*(10^-19));

                          (*Call f[] for Qp<->Pb, compute Vb*)
fb=f[x,t,nD,s,qb,kay];
rDb=(go+(1/r)*(1.6*10^-19)*(fb[[3]])*(fb[[5]]+fb[[2]])*0.0008)^-1;
vb=10.0*rDb*((rB+rDb)^-1);

                          (*Call f[] for Qp<->Pb+Ps,compute Vbs*)
fbs=f[x,t,nD,s,qb+qs,kay];
rDbs=(go+(1/r)*(1.6*10^-19)*(fbs[[3]])*(fbs[[5]]+fbs[[2]])*0.0008)^-1;
```

```
vbs=10.0*rDbs*((rB+rDbs)^-1);

                                    (*Evaluate resp[Pb+Ps]*)
sig=(vbs-vb)*10^6;
resp=(fb[[4]]*(vbs-vb))/(2.0*(10^-19)*aDet*qs);

                          (*Call f[] for Qp<->(1+10^-10)Pb,compute VbSS*)
qbSS=qb*(1.0000000001);
fbSS=f[x,t,nD,s,qbSS,kay];
rDbSS=(go+(1/r)*(1.6*10^-19)*(fbSS[[3]])*(fbSS[[5]]+fbSS[[2]])*0.0008)^-1;
vbSS=10.0*rDbSS*((rB+rDbSS)^-1);

                                    (*Evaluate small-signal resp*)
respSS=(fb[[4]]*(vbSS-vb))/(2.0*(10^-19)*aDet*((qbSS-qb)));

                                    (*Compute quantities of interest*)
b1=1/resp;
percentNL=((resp/respSS)-1)*100;
b2=((b1)^3)*100*(2.0*(10^-19)*aDet*qs)/(fb[[4]]*percentNL);
percenttau=((fbs[[1]]/fb[[1]])-1)*100;

                          (*Return list of results of interest to 6 place precision*)
N[{sig,resp,respSS,rDb,rDbs,qb,qs,t,pb,ps,percentN,percenttau,b1,b2},6]
]
```

To operate the code it is necessary that both f[] and perfP[] are evaluated, i.e. "loaded", into the Notebook or "routine" being run to do the calculations. The function perfP[] calls for output from f[].

APPENDIX C

ADDENDUM

During the completion of this report data from preliminary vacuum tests of the serial number 3(SNO3) Imager-3 detector became available. The data were collected with the detector in the instrument. The instrument responsivity was measured vs detector temperature.

This was of particular interest since the model predicted that the Imager 3 responsivity could increase over the detector operating temperature range with increasing detector temperature. (See Figure 10.) This behavior is somewhat counter-intuitive to the notion that HgCdTe detector's performance improves with decreasing temperature: In the case where detector responsivity dominates performance, the data indicate that this is not necessarily true, at least for all HgCdTe detectors.

A plot of the data(points) and the model fit(solid line) is shown in Figure C-1.

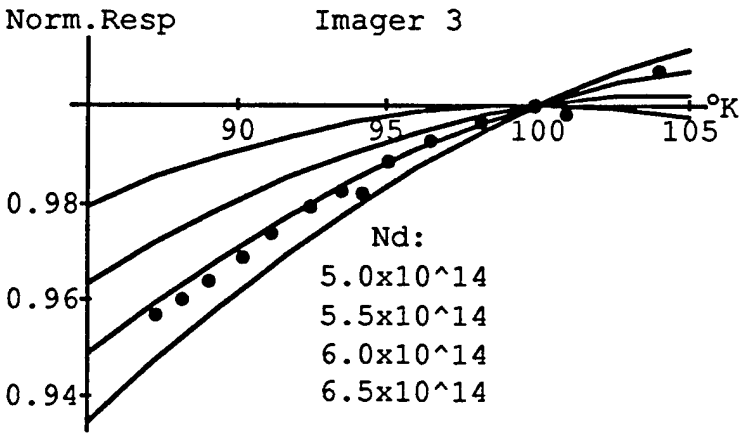

Figure C-1. Fit of Imager 3 model to in-situ instrument test data of normalized responsivity vs detector temperature. (Assumed background power, P_b =21nW.)

To fit the model the value of the impurity density, N_d(Table 1) was varied from the assumed $5x10^{14}/cm^3$ to $6.5x10^{14}/cm^3$. It can be seen from Figure C-1 that a value of $\approx 6x10^{14}/cm^3$ gives qualitative agreement. And it can be seen that the responsivity of Imager-3 does increase with increasing detector temperature over this range, as predicted by the model.

An explanation of this effect is given on pages 21-23 of the text. A consequence of the effect is that lowering in-orbit detector temperature may improve Sounder instrument performance in the Long-Wavelength bands, but may also slightly degrade Imager-3 performance.

The author appreciates Richard Heinrichs' providing a file of the test data.

ACRONYMS

A/D	Analog to Digital
AVHRR	Advanced Very High Resolution Radiometer
GOES -NEXT	New generation of GOES now being manufactured
GOES	Geosynchronous Operational Environmental Satellite
HgCdTe	Mercury Cadmium Telluride (alloy)
IFOV	Instantaneous Field of View
ITT	International Telephone and Telegraph (company)
LIRIS	Loral Infrared Imaging Systems (company)
LWIR	Long Wave Infrared Radiation
MIT/LL	Massachusetts Institute of Technology, Lincoln Laboratory
NASA	National Aeronautics and Space Administration
NEDN	Noise Equivalent Delta Radiance, Watt/cm^2-μm
NEDT	Noise Equivalent Delta Temperature, °K
NESDIS	National Environmental Satellite Data and Information Service
NOAA	National Oceanic and Atmospheric Administration
OGE	Operational Ground Equipment
PC	Photo-Conductive
SN03	Serial Number 3 (of GOES-NEXT)

REPORT DOCUMENTATION PAGE

Form Approved
OMB No. 0704-0188

1. AGENCY USE ONLY (*Leave blank*)	2. REPORT DATE	3. REPORT TYPE AND DATES COVERED
	17 May 2000	Project Report

4. TITLE AND SUBTITLE

HgCdTe Detector Responsibility and GOES Instrument Calibration

5. FUNDING NUMBERS

C — F19628-95-C-0002

6. AUTHOR(S)

W.E. Bicknell

7. PERFORMING ORGANIZATION NAME(S) AND ADDRESS(ES)

Lincoln Laboratory, MIT
244 Wood Street
Lexington, MA 02420-9108

8. PERFORMING ORGANIZATION REPORT NUMBER

PR-NOAA-3 (R-1)

9. SPONSORING/MONITORING AGENCY NAME(S) AND ADDRESS(ES)

Clarence Tignor
NOAA/SAO4, Room 10210
1315 East West Highway
SSMC 3
Silver Spring, MD 20910

10. SPONSORING/MONITORING AGENCY REPORT NUMBER

ESC-TR-99-065

11. SUPPLEMENTARY NOTES

None

12a. DISTRIBUTION/AVAILABILITY STATEMENT

Approved for public release; distribution is unlimited.

12b. DISTRIBUTION CODE

13. ABSTRACT (*Maximum 200 words*)

A model is developed for the responsivity of HgCdTe detectors employed in the GOES Sounder and Imager instruments. Response non-linearity is related to the calibrated radiometric accuracy of the instruments. The model, in the form of a computer code, could be utilized to expedite pre-launch calibration of GOES satellite instruments and to provide confidence in GOES in-orbit calibration procedures.

14. SUBJECT TERMS

15. NUMBER OF PAGES
60

16. PRICE CODE

17. SECURITY CLASSIFICATION OF REPORT	18. SECURITY CLASSIFICATION OF THIS PAGE	19. SECURITY CLASSIFICATION OF ABSTRACT	20. LIMITATION OF ABSTRACT
Unclassified	Unclassified	Unclassified	Unclassified